an anisotropy of about a factor of 6.5 in the κ parameter of type-II superconductivity.[11] One peculiar property of superconducting $(TMTSF)_2PF_6$ is that three-dimensional shielding currents are reduced in magnitude in very low applied fields, which means that the critical supercurrent density must be very low in at least two directions, probably transverse to the chain axis. From all our T_c vs P data we find a strong dependence of T_c on pressure, as is shown in Fig. 4.

In conclusion, we have shown that $(TMTSF)_2PF_6$ under pressure is a bulk superconductor in near-zero field which exhibits rather unusual and very anisotropic properties in applied fields. We wish to thank P. W. Anderson, E. I. Blount, and C. M. Varma for helpful comments.

[1]K. Bechgaard, C. S. Jacobsen, K. Mortensen, H. J. Pedersen, and N. Thorup, Solid State Commun. 33, 1119 (1980).

[2]*The Physics and Chemistry of Low Dimensional Solids*, edited by L. Alcacer (Reidel, Hingham, Mass., 1980).

[3]D. Jerome, A. Mazaud, M. Ribault, and K. Bechgaard, J. Phys. Lett. 41, L95 (1980).

[4]M. Ribault, G. Benedek, D. Jerome, and K. Bechgaard, J. Phys. Lett. 41, L397 (1980).

[5]J. Bardeen, L. N. Cooper, and J. R. Schrieffer, Phys. Rev. 108, 1175 (1957).

[6]H. Fröhlich, Proc. Roy. Soc. London, Sect. A 223, 296 (1954).

[7]P. W. Anderson, P. A. Lee, and M. Saitoh, Solid State Commun. 13, 595 (1973).

[8]D. Allender, J. W. Bray, and J. Bardeen, Phys. Rev. B 9, 119 (1974).

[9]P. A. Lee and T. M. Rice, Phys. Rev. B 19, 3970 (1979), and references therein.

[10]W. A. Little, Phys. Rev. 134, A1416 (1964).

[11]See, for example, *Superconductivity*, edited by R. D. Parks (Dekker, New York, 1969).

[12]C. W. Chu, L. R. Testardi, F. J. Di Salvo, and D. E. Moncton, Phys. Rev. B 14, 464 (1976).

[13]In both the shielding and Meissner signals of this sample and the resistivity of a similar sample, we see evidence of two transition temperatures, a sharp one at 0.7 K and a broader one below 0.6 K. K. Andres, F. Wudl, D. B. McWhan, G. A. Thomas, D. Nalewajek, and A. L. Stevens, to be published.

Island Growth and Orientational Locking of Potassium Intercalated in Graphite

A. N. Berker,[a] N. Kambe,[b] G. Dresselhaus,[c] and M. S. Dresselhaus[b]
Center for Materials Science and Engineering, Massachusetts Institute of Technology, Cambridge, Massachusetts 02139
(Received 29 April 1980)

Island growth and orientational locking in stage-2 potassium-intercalated graphite is observed by real-space imaging and electron diffraction on single crystallites. A mechanism is presented, relating these two phenomena. For $86 \lesssim T \lesssim 130$ K, intercalate islands of incommensurate ordering are orientationally unlocked from the graphite lattice, as indicated by ring diffraction patterns. With increasing temperature, gradual island growth is by accretion. A threshold size (~ 50 Å reached at 130 K) triggers precipitous island growth by coalescence and orientational locking.

PACS numbers: 81.30.Hd, 61.16.Di, 64.70.Kb, 68.55.+b

Intercalate systems, in addition to their inherent materials science interest, provide a new arena for the study of phase transitions and critical phenomena, involving a large variety of possible phases[1] and, presumably, new phenomena where these phases meet. Whereas recent studies[2-4] of these systems have almost uniformly interpreted experimental data in terms of single homogeneous phases, this Letter describes, for stage $n = 2$ potassium in graphite, the necessary and interesting coexistence of distinct regions which differ in intercalate concentration and structure. We report electron diffraction measurements which probe a single graphite crystallite within highly oriented pyrolytic graphite, in the temperature range of $5 < T < 800$ K. These measurements are supplemented by bright-field and dark-field real-space images of the crystallite. The experiments show, for intermediate[5] temperatures $86 < T < 130$ K, the occurrence of small "islands" of positional order incommensurate[6] to graphite basal structure, in a "sea" of disorder. These islands are orientationally unlocked from the graphite and, therefore, from each other, as indicated by a diffraction pattern of six to eight discernible sharp rings [Fig. 1(b)], which are

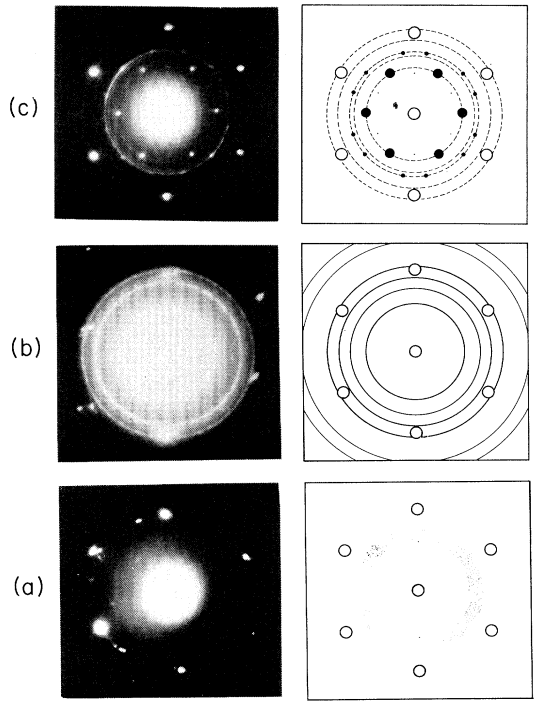

FIG. 1. Electron diffractograms of postassium-intercalated graphite at (a) 13 K, (b) 118 K, and (c) 305 K. On the right is a schematic illustration of each diffractogram.

indexed and structurally identified (Table I). Above $T_u = 130$ K, larger islands orientationally lock onto the graphite, as indicated by diffraction spots exactly superimposed on the rings which persist because of the smaller unlocked islands. A mechanism for this phenomenon is presented.

Our observations were carried out starting with stage-2 potassium-intercalated graphite, characterized by $(00l)$ x-ray diffractograms. Results were *reversible* with respect to heating and cooling cycles below room temperature. From $(00l)$ integrated intensities, identically prepared materials yielded[7] a composition of approximately $C_{21}K$, which already suggests the possibility of coexisting phases. Electron diffraction is sensitive to $(hk0)$ reciprocal-lattice points, giving detailed information about in-plane ordering. Bright-field images give information about in-plane homogeneity including changes in domain size at a phase transition. Use of liquid-helium- and liquid-nitrogen-cooled stages and a heating assembly[8] provided the temperature range $5 < T < 800$ K.

In the temperature range of 5 to 800 K, three regimes are seen,[5] separated by $T_l \simeq 86$ K and $T_u \simeq 130$ K. Representative diffraction patterns are in Fig. 1. Below T_l, we infer the coexistence of a $\sqrt{3} \times \sqrt{3}$ commensurate ordered phase (denoted by C_3), previously reported,[9] and a disordered phase (D). The $\sqrt{3} \times \sqrt{3}$ phase has c-axis correlation with an $\alpha\beta\gamma$ stacking, so that the structure factor for the $(hk0)$ superlattice vanishes exactly.[8,10] Accordingly, only the 1×1 spots are observed in Fig. 1(a). From the broad ring in Fig. 1(a), as well as from a quantitative (density $\rho_D > \frac{1}{7}$) argument given below, it is concluded that the disordered phase contains substantial amounts of intercalant.

In similar recent studies[8] of cesium and rubidium in graphite, the $\sqrt{7} \times \sqrt{7}$ phase plays the role of the $\sqrt{3} \times \sqrt{3}$ phase in potassium-intercalated graphite. With the Cs and Rb compounds, the $\sqrt{7} \times \sqrt{7}$ superlattice spots are clearly seen by electron diffraction. This contrast can be understood, since a sevenfold ordered repetition ($\alpha\beta\gamma\delta\epsilon\zeta\eta$!) would require interactions across $6n$ graphite planes. We have in fact observed the $\sqrt{7} \times \sqrt{7}$ spots in potassium-intercalated graphite below T_l in rare instances. This additional information will be sensible in view of the region above T_l.

Above T_l, sharp ring patterns are obtained from electron diffraction [Fig. 1(b)]. Simultaneously, the graphite spots remind us that the signal comes from a single crystallite. This, in conjunction with the real-space images to be discussed below, is explained by the existence of small islands of positional order incommensurate to the graphite basal structure, surrounded by the disordered phase D. These islands are orientationally unlocked from the graphite and, therefore, from each other. Hence, instead of a spot pattern, rings with temperature-dependent diameters are obtained. These are indexed and their q values given in Table I, yielding dilated $\sqrt{3} \times \sqrt{3}$ and contracted $\sqrt{7} \times \sqrt{7}$ structures (respectively, denoted by I_3 and I_7). For example, whereas the perfect $\sqrt{3} \times \sqrt{3}$ and $\sqrt{7} \times \sqrt{7}$ nearest-neighbor distances are 4.26 and 6.51 Å, the ring patterns at $T \gtrsim T_l$ indicate 4.62 and 5.52 Å.

Above T_u, distinct spot patterns are seen exactly superimposed onto the rings [Fig. 1(c)]. This novel observation is explained in terms of precipitous island growth and orientational locking triggered by the substrate potential at a critical island size (~50 Å). Figure 2 shows bright-field, real-space images of the sample. X-ray fluorescence measurements at 300 K indicate that the darker regions are richer in potassium. Dark-field real-space images indicate that the I_3 dif-

TABLE I. Identification of incommensurate structures from locations of diffraction peaks, given in inverse angstroms. In the interval $T_l \simeq 86$ K$\lesssim T \lesssim T_u \simeq 130$ K, the ring patterns evolve between the two limits given below. This suggests that the peripheries of the I_3 and I_7 islands deviate toward the intermediate density of D. The importance of the peripheries decreases as islands grow with increasing T.

Calculated wave vectors	Electron diffraction $T \gtrsim T_l$	X-ray diffraction[a]	Electron diffraction $T \lesssim T_u$	Calculated wave vectors
1.32[b]		(1.26)	1.28 ± 0.02	1.26[c]
1.57[d]	1.63 ± 0.04	1.70	1.78 ± 0.08	1.80[e]
2.28[b]	2.19 ± 0.05	2.18	2.18 ± 0.05	2.18[c]
		(2.40)		
2.63[b]	2.65 ± 0.06	(2.75)	2.61 ± 0.03	2.52[c]
2.72[d]	2.65 ± 0.06	(3.13)	2.96 ± 0.06	3.11[e]
3.14[d]	3.16 ± 0.09	3.66	3.71 ± 0.10	3.59[e]
3.48[b]		(3.25)	3.29 ± 0.12	3.33[c]
	3.71 ± 0.01			
3.94[b]	3.96 ± 0.01	3.86	3.71 ± 0.10	3.78[c]
4.16[d]	4.16 ± 0.04		4.78 ± 0.03	4.75[e]
4.55[b]	4.52 ± 0.06	4.22	4.35 ± 0.06	4.36[c]
4.71[d], 4.74[b]	4.72 ± 0.05			4.54[c]

[a]Ref. 3. Parenthesized peaks are our reading of data in Fig. 2 of Ref. 3. No variation in the peak locations with T is reported.
[b]I_7 with lattice constant $a = 5.52$ Å with unweighed residual $R = 0.030$.
[c]I_7 with $a = 5.76$ Å with $R = 0.027$.
[d]I_3 with $a = 4.62$ Å with $R = 0.024$.
[e]I_3 with $a = 4.04$ Å with $R = 0.043$. Note this fit is less satisfactory.

fraction rings come from the darkest regions in Fig. 2. Below T_u, Fig. 2(a) shows numerous black (I_3) and white (I_7) islands of characteristic size of 33 Å against a background of gray (D), which supports the previous paragraph. An island of incommensurate positional order can reduce internal energy by orientationally aligning with the graphite planes.[11] This energy reduction should be roughly proportional to the area of the island. Thus, at temperature T, for a given I_3 island of area $A(T)$ and orientation θ, a partition function can be written,

$$Z(\text{orient}) = (1/2\pi)\int_0^{2\pi} d\theta \exp\{[\mathfrak{C}A(T)/kT]\cos 6\theta\},$$

where $\mathfrak{C} > 0$ is a constant and $-\mathfrak{C}A(T)$ is the substrate field for orienting the island. [For an I_7 island $\cos 6\theta$ is replaced by[8] $\cos 6\theta - 0.60\cos 12\theta$, but the same argument applies.] Unlike the energy, the entropy due to nonalignment is roughly independent of the island size. Thus, in the small-size limit, nonalignment is favored. The islands of given intermediate size have a distribution around $\langle\cos 6\theta\rangle = 1$ with a spread $\langle\cos^2 6\theta\rangle - \langle\cos 6\theta\rangle^2 = 1 - I_1/xI_0 - I_1^2/I_0^2$, where the argument of the Bessel functions $I_{0,1}$ is $x \equiv \mathfrak{C}A(T)/kT$. This is the type of alignment of a paramagnet in an external field, $\mathfrak{C}A(T)$, which is weak enough not to be discernible on the rings of Fig. 1(b). However, consider the experimental scan, indicated by the dashed line in Fig. 3, in the coexistence region $I + D$. As temperature is gradually increased, if the boundary of the coexistence region on the I side is approached, as depicted in Fig. 3, the islands can be expected to grow gradually by accretion. *Both* the I_3 and I_7 islands must grow and the density ρ_D of D must be between the densities of I_3 and I_7, $\frac{1}{3} \gtrsim \rho_D \gtrsim \frac{1}{7}$, if overall density is to be conserved. This is consistent with the shading of the bright-field images. If $A(T)$ grows faster than T, alignment increases as temperature increases, the spread decreasing as $kT/\mathfrak{C}A(T)$. It is much easier to span a bridge between two neighboring islands when they both achieve a certain alignment. This is the phenomenon behind epitaxial crystal growth. Bridging causes precipitous island growth by coalescence, which in turn sharply increases alignment. A runaway process is thus triggered beyond a threshold size.

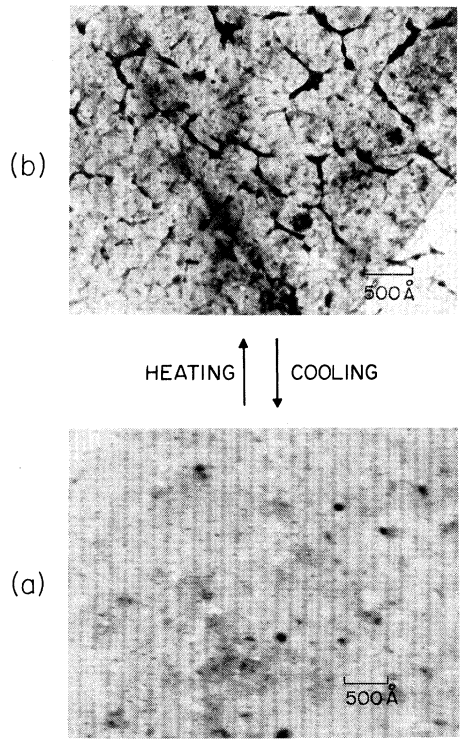

FIG. 2. Bright-field images of potassium-intercalated graphite at 118 and 293 K, showing dense black islands (I_3), dilute white islands (I_7), and intermediate-density gray background (D).

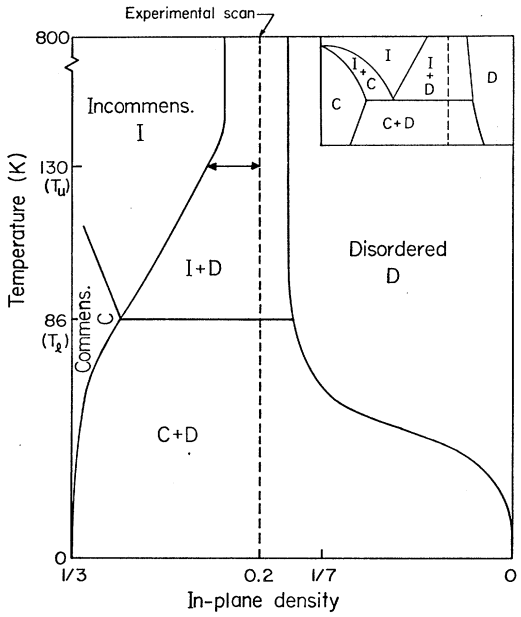

FIG. 3. Possible phase diagram of stage-2 potassium-intercalated graphite, shown schematically. This is the simplest phase diagram consistent with our experimental results obtained along the temperature scan represented by the dashed line. The commensurate-incommensurate transition on the left can be a priori either second order (main frame), or first order (inset), respectively, corresponding to either a critical end point, or a triple point at T_l.

The result is large islands, their oblong shapes reflecting their creation by the coalescence of units which have independently reached threshold size. This is indeed seen above T_u [Fig. 2(b)]. This runaway growth orientationally locks the islands onto the graphite and, therefore, onto each other, giving the diffraction *spots*. The smaller unlocked, uncoalesced islands (as well as the smaller peninsulas, unlocked because of weak connections to the larger entity) sustain the diffraction *rings*. Since both categories of this bimodal distribution,[8] though orientationally distinct, share the same positional character, the spots are exactly superimposed onto the rings. As seen in Fig. 2(b), the coalesced islands even tend towards percolating throughout the sample, to form a macroscopic domain. This major structural rearrangement which enters our explanation of T_u is consistent with reported transport-property anomalies.[5]

We thank Dr. H. Mazurek and Dr. A. J. Garratt-Reed for help with scanning transmission electron microscopy measurements, and Professor R. B. Griffiths for discussions. This research has been supported by the National Science Foundation under Grant No. 78-10858.

[a]Also at Department of Physics.
[b]Also at Department of Electrical Engineering and Computer Science.
[c]Also at Francis Bitter National Magnet Laboratory.

[1]G. S. Parry and D. E. Nixon, Nature (London) 216, 909 (1967); G. S. Parry, Mater. Sci. Eng. 31, 99 (1977).
[2]J. B. Hastings, W. D. Ellenson, and J. E. Fischer, Phys. Rev. Lett. 42, 1552 (1979).
[3]H. Zabel, S. C. Moss, N. Caswell, and S. A. Solin, Phys. Rev. Lett. 43, 2022 (1979).
[4]R. Clarke, N. Caswell, S. A. Solin, and P. M. Horn, Phys. Rev. Lett. 43, 2018 (1979), and Physica (Utrecht) 99B, 457 (1980).
[5]D. G. Onn, G. M. T. Foley, and J. E. Fischer, Phys. Rev. B 19, 6474 (1979).
[6]B. I. Halperin and D. R. Nelson, Phys. Rev. Lett. 41, 121 (1978).
[7]S. Y. Leung, C. Underhill, G. Dresselhaus, T. Krapchev, R. Ogilvie, and M. S. Dresselhaus, Solid State Commun. 32, 635 (1979).
[8]N. Kambe, G. Dresselhaus, and M. S. Dresselhaus,

Phys. Rev. B 21, (1980), and to be published.
[9]E. L. Evans and J. M. Thomas, J. Solid State Chem. 14, 89 (1975).
[10]N. Kambe, M. S. Dresselhaus, G. Dresselhaus, S. Basu, A. R. McGhie, and J. E. Fischer, Mater. Sci. Eng. 40, 1 (1979).
[11]A. D. Novaco and J. P. McTague, Phys. Rev. Lett. 38, 1286 (1977).

Fractal Form of Proteins

H. J. Stapleton, J. P. Allen, C. P. Flynn, D. G. Stinson, and S. R. Kurtz
Department of Physics and Materials Research Laboratory, University of Illinois at Urbana-Champaign, Urbana, Illinois 61801
(Received 20 March 1980)

Electron spin relaxation measurements on low-spin Fe^{3+} in several proteins show that they occupy a space of fractal dimensionality $d = 1.65 \pm 0.04$, in conformity with the dimensionality $d = \frac{5}{3}$ of a self-avoiding random walk. Analysis of myoglobin x-ray data independently confirms this fractal dimension.

PACS numbers: 87.15.By, 63.50.+x, 76.30.-v

We report the temperature dependence of the electron spin relaxation rate of low-spin Fe^{3+} in myoglobin azide (MbN_3) and ferricytochrome *c* (CC). We also reanalyze other relaxation data from two low-spin hemoproteins: cytochrome P-450 from pseudomonas putida (CP 450), originally reported by Herrick and Stapleton[1] (denoted by I), and CC.[2] All systems have been studied as frozen aqueous solutions, but single crystals were used in the earlier CC work.[2] Unlike its high-spin counterpart, low-spin iron has no low-lying excited electronic states. The direct and Raman relaxation rates, which in three-dimensional materials vary with temperature T as AT and CT^9, respectively, are therefore not masked by an Orbach (resonant Raman) process.[3] The temperature dependence of the Raman rate measures the density of states in the vibrational spectrum of the material. All our relaxation data are consistent with a Raman rate of the form $CT^{6.30\pm0.07}$, with C a constant. The density $\rho(\omega)$ of vibrational states therefore varies with frequency as $\omega^{0.65\pm0.04}$. We deduce that the protein has the form of a fractal[4] of dimensionality 1.65 ± 0.04. Within the experimental uncertainties this is identical with the fractal dimensionality $d=\frac{5}{3}$ of the self-avoiding random walk (SAW),[4] to which the protein backbone bears a marked resemblance.

The relaxation rates of MbN_3 and CC were measured directly at 9.5 GHz between 1.5 and 10 K with use of the pulse saturation and recovery technique, with a superheterodyne receiver and fast microwave diode switches. These measurements were limited to rates under 10^4 s^{-1}. The temperature readout and control were accurate to a few millidegrees Kelvin. More experimental details are given in I. Data of Mailer and Taylor for CC were obtained by measuring the phase lag of the magnetic resonance signal under conditions of adiabatic fast passage.[2] These measurements yielded relaxation rates at temperatures between 11 and 18 K.

The Raman relaxation mechanism is a two-phonon process in which a paramagnetic spin flips; one quantum of vibrational energy at ω_1 is destroyed and another at ω_2 created, with $\hbar(\omega_2 - \omega_1) = g\mu_B H$. At temperatures for which this mechanism is dominant over the direct (one-phonon) relaxation mechanism one can take $\omega_1 = \omega_2$ to obtain the temperature dependence of the Raman rate as

$$\frac{1}{T_{1R}} \propto \int_0^{\omega_{max}} \rho^2(\omega)\omega^4 f(\hbar\omega/kT)d\omega\,, \qquad (1)$$

with $\rho(\omega)$ the density of vibrational states and $f(z) = e^z/(e^z-1)^2$. The creation of one, and the destruction of another, vibrational quantum introduces two of the four powers of ω into Eq. (1). The remaining two powers must be present if the interaction is electrostatic in nature and the ion possesses an odd number of electrons.[3]

If we postulate a power law $\rho(\omega) \propto \omega^p$ for the density of states, the Raman rate of Eq. (1) must vary with temperature T as

$$\frac{1}{T_{1R}} \propto \left(\frac{kT}{\hbar}\right)^{5+2p} F_{4+2p}(\Theta/T)\,. \qquad (2)$$

Here $\Theta \equiv \hbar\omega_{max}/k$ and $F_{4+2p}(\Theta/T)$ is a function

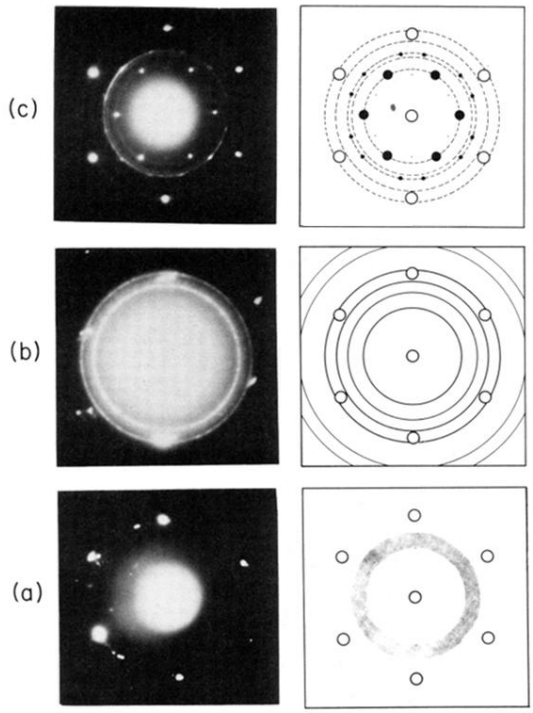

FIG. 1. Electron diffractograms of postassium-intercalated graphite at (a) 13 K, (b) 118 K, and (c) 305 K. On the right is a schematic illustration of each diffractogram.

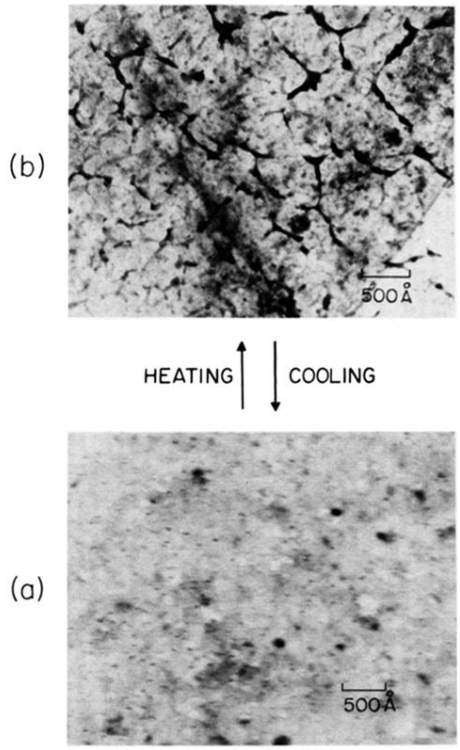

FIG. 2. Bright-field images of potassium-intercalated graphite at 118 and 293 K, showing dense black islands (I_3), dilute white islands (I_7), and intermediate-density gray background (D).